

# Unusual void galaxy DDO 68: implications of the *HST*-resolved photometry

D. I. Makarov,<sup>1\*</sup> L. N. Makarova,<sup>1†</sup> S. A. Pustilnik<sup>1‡</sup> and S. B. Borisov<sup>2,3</sup>

<sup>1</sup> *Special Astrophysical Observatory of RAS, Nizhnij Arkhyz, Karachai-Cherkessian Republic, 369167, Russia*

<sup>2</sup> *Sternberg Astronomical Institute, Moscow State University, Moscow, 119991, Russia*

<sup>3</sup> *Department of Physics, Moscow State University, 1, Leninskie Gory, Moscow, 119991, Russia*

14 October 2018

## ABSTRACT

DDO 68 (UGC 5340) is an unusual dwarf galaxy with extremely low gas metallicity [ $12 + \log(\text{O}/\text{H}) = 7.14$ ] residing in the nearby Lynx–Cancer void. Despite its apparent isolation, it shows both optical and H I morphological evidence for strong tidal disturbance. Here, we study the resolved stellar populations of DDO 68 using deep images from the *HST* archive. We determined a distance of  $12.75 \pm 0.41$  Mpc using the tip of the red giant branch (TRGB). The star formation history reconstruction reveals that about 60 per cent of stars formed during the initial period of star formation, about 12–14 Gyr ago. During the next 10 Gyr, DDO 68 was in the quenched state, with only slight traces of star formation. The onset of the most recent burst of star formation occurred about 300 Myr ago. We find that young populations with ages of several million to a few hundred million years are widely spread across various parts of DDO 68, indicating an intense star formation episode with a high mean rate of  $0.15 M_{\odot} \text{ yr}^{-1}$ . A major fraction of the visible stars in the whole system ( $\sim 80$  per cent) have low metallicities:  $Z = Z_{\odot}/50$ – $Z_{\odot}/20$ . The properties of the northern periphery of DDO 68 can be explained by an ongoing burst of star formation induced by the minor merger of a small, gas-rich, extremely metal-poor galaxy with a more typical dwarf galaxy. The current TRGB-based distance of DDO 68 implies a total negative peculiar velocity of  $\approx 500 \text{ km s}^{-1}$ .

**Key words:** galaxies: dwarf – galaxies: stellar content – galaxies: evolution – galaxies: interactions – galaxies: individual: DDO 68 (UGC 5340)

## 1 INTRODUCTION

The unusual dwarf irregular galaxy DDO 68 (UGC 5340) is located in the nearby Lynx–Cancer void (Pustilnik & Tepliakova 2011). Recent distance estimations place DDO 68 between 12 and 13 Mpc (Cannon et al. 2014; Tikhonov et al. 2014). The galaxy has a large negative peculiar velocity of about  $-500 \text{ km s}^{-1}$ . This is  $\sim 200 \text{ km s}^{-1}$  larger than the prediction of the velocity-field model in this region by Tully et al. (2008).

Despite its apparent isolation, DDO 68 shows a peculiar morphology: several prominent star-forming regions on the periphery, mainly in the ‘northern ring’ and the ‘southern tail’ (Pustilnik et al. 2005). The H I study with the Giant Meterwave Radio Telescope (GMRT; Ekta, et al. 2008), as

well as less sensitive observations with the Westerbork Synthesis Radio Telescope (Stil & Israel 2002), show the complex gas structure and the velocity field consisting of two arms, winding asymmetrically around the main bright part of the optical body. Ekta, et al. (2008) suggest that DDO 68 is likely the result of a merging of two gas-rich dwarfs. The recent very deep H I study with the Very Large Array and the Green Bank Telescope revealed a faint interacting companion DDO 68C at a projected distance of 42 kpc from DDO 68. The optical counterpart of the companion is hidden in the halo of a bright star, preventing direct stellar mass measurement. It was found that its gas mass is smaller than that of DDO 68 by a factor of  $\sim 35$  (Cannon et al. 2014). Annibali et al. (2016) concluded that the disturbed morphology of DDO 68 and its nearby tidal features cannot be explained by the influence of DDO 68C.

DDO 68 has an extremely low gas-phase oxygen abundance of  $12 + \log(\text{O}/\text{H}) = 7.14$ – $7.20$ . The current O/H-value is based on direct measurements by the classic

\* E-mail: dim@sao.ru (DIM)

† E-mail: lidia@sao.ru (LNM)

‡ E-mail: sap@sao.ru (SAP)

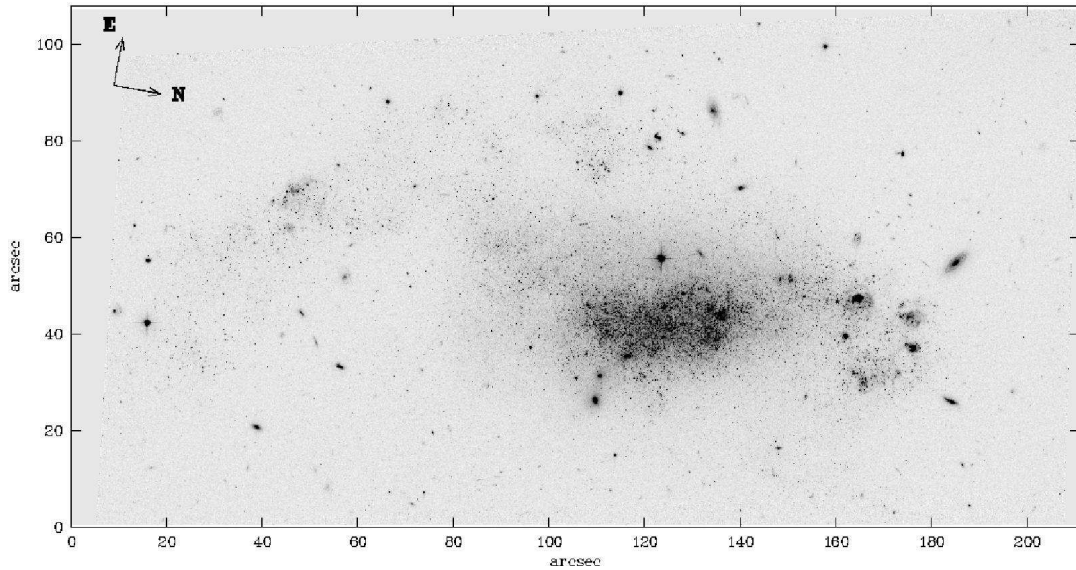


**Figure 1.** The *HST*/*ACS* image of DDO 68 in the *F606W* filter. Only WFC1 detector field is shown.

$T_e$ -method of the several brightest H II regions in the ‘northern ring’ (Pustilnik et al. 2005; Izotov & Thuan 2007; Berg et al. 2012; Izotov et al. 2012). Along with its void ‘neighbour’ SDSS J0926+3343 with  $12 + \log(\text{O}/\text{H}) = 7.12$  (Pustilnik et al. 2010) and the recently discovered very faint neighbour of the Local Group, Leo P, with  $12 + \log(\text{O}/\text{H}) = 7.17$  (Skillman et al. 2013), DDO 68 is considered as one of the most metal-poor galaxies in the Local Volume and its surroundings. A prototype extremely low metallicity blue compact galaxy I Zw 18 has  $12 + \log(\text{O}/\text{H}) = 7.16\text{--}7.19$  (e.g., Skillman & Kennicutt 1993; Izotov & Thuan 1998, and references therein). It is somewhat farther, with distance estimates from  $D \sim 15$  to 19 Mpc (Izotov & Thuan 2004; Contreras Ramos et al. 2011). A couple of new, nearby, extremely metal-deficient dwarfs, UGC 772 and SDSS J1056+3608, with  $12 + \log(\text{O}/\text{H}) \sim 7.16$  were presented by Izotov et al. (2012). The galaxy SBS 0335–052W has the lowest known metallicity  $12 + \log(\text{O}/\text{H}) \sim 6.9$  (Izotov et al. 2009). However, it is a significantly more distant object, with a distance of about 54 Mpc.

Pustilnik & Tepliakova (2011) emphasize the high concentration of very-low-metallicity dwarfs in the Lynx–Cancer void. Recently, Hirschauer et al. (2016) discovered the record-low metallicity for the dwarf galaxy SDSS J094332.35+332657.6 [ $12 + \log(\text{O}/\text{H}) = 7.02 \pm 0.03$ ] identified with the H I-source AGC 198691, which was found within the framework of the blind H I Arecibo Legacy Fast ALFA Survey (Haynes et al. 2011). One more extremely metal-poor dwarf galaxy J0706+3020 with ( $12 + \log(\text{O}/\text{H}) = 7.03$ ) was found near the centre of the void (Chengalur et al. 2016; Pustilnik et al. 2016b). These findings reinforce the conclusion of Pustilnik & Tepliakova (2011) on the high concentration of very metal-poor galaxies in voids. At a kinematic distance of  $\sim 10.8$  Mpc, AGC 198691 appears to be a neighbour of both extremely low-metallicity galaxies, SDSS J0926+3343 and DDO 68.

Using the *Hubble Space Telescope* (*HST*) archive data, Tikhonov et al. (2014) distinguish two very different spatial components of the resolved stellar populations in DDO 68.

The population with medium metallicity ( $Z_{\odot}/5$ ) is concentrated in the central high density part of the galaxy. The low-metallicity component ( $Z \lesssim Z_{\odot}/20$ ) winds around the main body from the ‘northern ring’ to the ‘southern tail’. The authors found that the secondary component has only a small fraction of old stars, as opposed to the case of the main body.

In the course of revising our paper, Sacchi et al. (2016) published their article on the star formation history (SFH) reconstruction in DDO 68. They conclude that almost 80 per cent of the total stellar mass ( $M_{*} \simeq 1.3 \times 10^8 M_{\odot}$ ) comprises of old (age  $> 1$  Gyr) stars. This result allows the authors to reject the hypothesis that DDO 68 is a young system experiencing its first burst of star formation.

In this work, we concentrate on the general study of stellar populations of DDO 68 using the deep images from the *HST* archive. We examine the distribution of stars of different ages and metallicities throughout the galaxy. We reconstruct the SFH in different regions of DDO 68 using the Padova theoretical isochrones of stellar evolution (Girardi et al. 2000). We determine the distance modulus with the improved tip of the red giant branch (TRGB) method (Makarov et al. 2006) and calibration (Rizzi et al. 2007).

In a complementary paper (Pustilnik et al. 2016a), we analyse the variability of the known luminous blue variable in DDO 68 (Pustilnik et al. 2008; Izotov & Thuan 2009). Using the *HST* H  $\alpha$  images, high-resolution GMRT H I observations, and the Russian 6-m telescope’s Fabry–Perot interferometer data we address properties of the giant supershell and ionized gas shells related to the regions of recent star formation in the galaxy. We also present a subsample of the most luminous stars with the assumed record-low metallicities.

## 2 OBSERVATIONAL DATA AND REDUCTION

DDO 68 was observed with the *HST* using the Advanced Camera for Surveys (ACS; GO 11578, PI A. Aloisi). Deep images were obtained with the broad-band filters *F606W* (7644s) and *F814W* (7644s). Also, the galaxy was observed with the narrow-band filter *F658N* centred at  $H\alpha$  (2388s). The ACS image in *F606W* filter is shown in Fig. 1.

We use the ACS module of the DOLPHOT<sup>1</sup> software package by Dolphin (2002) to perform the photometry of the resolved stars as well as to run artificial star tests to characterize the completeness and uncertainties in the measurements. The data quality images were used to mask bad pixels. Only stars with photometry of a good quality were used in the analysis. We have selected about 36000 stars with a signal-to-noise of at least 5 in both filters and  $|\text{sharp}| \leq 0.3$ . The resulting colour–magnitude diagram (CMD) in *F606W* – *F814W* versus *F814W* is plotted in Fig. 2.

## 3 ANALYSIS

### 3.1 Colour–magnitude diagram

The CMD of DDO 68 is typical for a dwarf irregular galaxy with ongoing star formation. The highly populated upper part of the main sequence (MS), blue supergiants, has a mean colour index close to zero, while the red supergiants (RSG) and the young asymptotic giant branch (AGB) stars, as well as the middle-age AGB stars have a colour index  $(F606W - F814W) \gtrsim 0.9$  and an *F814W* magnitude brighter than 26.5. The deep images allow us to resolve the most densely populated red giant branch (RGB), which is visible at the bottom of the diagram [ $(F606W - F814W) \gtrsim 0.5$  and  $F814W \gtrsim 26.5$ ]. We estimate the distance modulus to be equal to  $30.53 \pm 0.07$  mag corresponding to a distance of  $12.75 \pm 0.41$  Mpc (see Section 3.2).

Because DDO 68 has a complex morphology, for further analysis we distinguish several parts of the galaxy: ‘head’, ‘body’, ‘middle’, ‘tail’ (see Fig. 3). The ‘head’ (in our notation) includes the ‘northern ring’ and the ‘tail’ coincides with the ‘southern tail’, named by Pustilnik et al. (2005). Deep photometry of resolved stars allows us to study the variation of the stellar populations in each part in sufficiently high detail. We analyse the CMD of the entire galaxy as well as of each part separately. Fig. 4 shows that the distribution of the resolved stellar populations is very inhomogeneous over the galaxy body. The ‘head’ is clearly dominated by blue stars. The ‘body’ shows some excess of bright blue and red supergiants. The ‘tail’ mostly has a considerable excess of blue but fainter stars ( $F814W \gtrsim 26$  mag). The ‘middle’ part reveals a clear dominance of red giants and AGB stars. This difference clearly demonstrates a complex evolution of the galaxy in time and may also favour the hypothesis of DDO 68 formation through a merger of two dwarf galaxies.

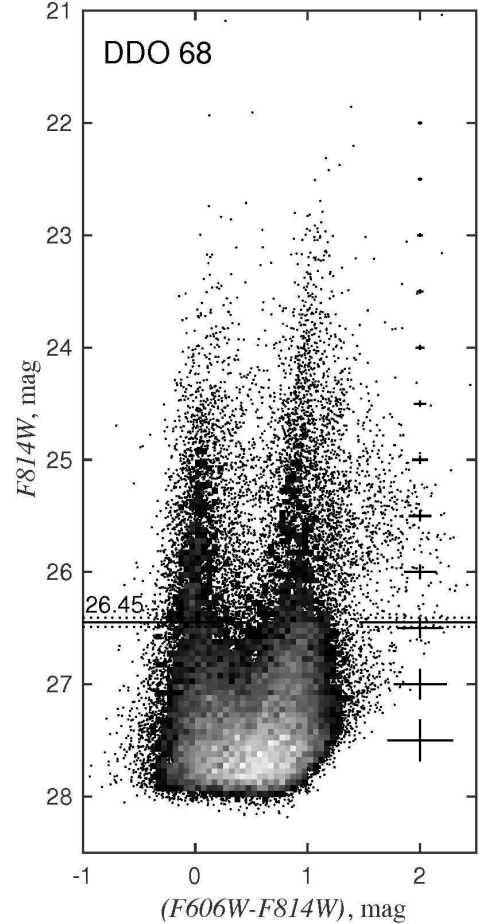


**Figure 2.** The colour–magnitude diagram of 35786 stars in DDO 68 in the *HST*/ACS flying system. The illustration combines a simple plot of individual stars as dots and a Hess diagram for the most dense regions in grey-scale, where the denser bin is lighter.

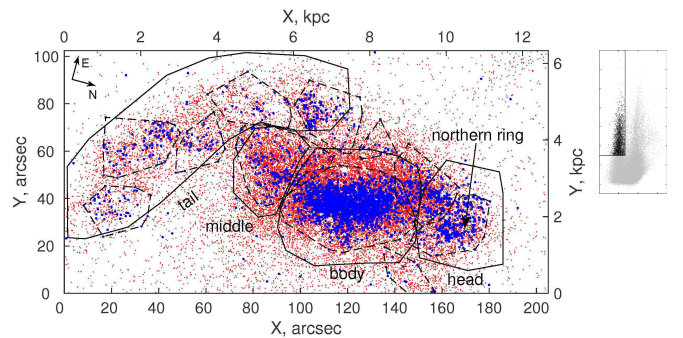


**Figure 3.** Distribution of stars in DDO 68. Blue points correspond to the bright blue part of the main sequence with  $(F606W - F814W) < 0.33$  and  $F814W < 26.5$  mag, which is highlighted in the CMD at the right. Small red dots show the rest of the DDO 68 stellar populations. Concentrations of young main-sequence stars are encircled by dashed lines. The four main regions of DDO 68 considered in the paper are delineated by solid lines and marked by their designations.

<sup>1</sup> <http://americano.dolphinim.com/dolphot>



### 3.2 Distance determination

The precise distance is a crucial point for the determination of the physical properties of a galaxy, and, in particular, for the SFH analysis. [Makarova & Karachentsev \(1998\)](#) measured a distance of 5.9 Mpc using the brightest blue stars in DDO 68. Later, [Pustilnik & Tepliakova \(2011\)](#) increased it to 9.9 Mpc based on the model of the velocity field in the local Universe ([Tully et al. 2008](#)). Recently, [Tikhonov et al. \(2014\)](#) shifted the galaxy significantly farther away to  $12.0 \pm 0.3$  Mpc using the TRGB methodology proposed by [Lee et al. \(1993\)](#). [Cannon et al. \(2014\)](#) received even slightly higher TRGB distance of  $12.74 \pm 0.27$  Mpc, but without a specification of the used calibration. [Sacchi et al. \(2016\)](#) found a TRGB modulus of  $(m - M)_0 = 30.41 \pm 0.12$  ( $D = 12.08 \pm 0.67$  Mpc) using the relation between TRGB magnitude and metallicity by [Bellazzini et al. \(2004\)](#). However, they adopt the slightly higher distance modulus  $(m - M)_0 = 30.51$ , or  $D = 12.65$  Mpc, as required by the fit of the observations by the synthetic CMD. The last three TRGB measurements are based on the same deep *HST*/ACS images of DDO 68 from the *HST* archive (proposal 11578, PI A. Aloisi).

We reprocessed these data independently with the TRG-BTOOL program, which uses a maximum-likelihood algorithm for TRGB determination from the luminosity function of the resolved stellar populations ([Makarov et al. 2006](#)). We derived the tip value of  $F814W = 26.448 \pm 0.040$  mag in the ACS instrumental system. The corresponding colour at the position of the TRGB is  $(F606W - F814W)_{\text{TRGB}} = 0.977 \pm 0.007$  mag. Taking into account the galactic colour excess  $E(B - V) = 0.0183$  from [Schlegel et al. \(1998\)](#), we derived the true distance modulus of DDO 68,  $(m - M)_0 = 30.527 \pm 0.070$  mag. It corresponds to the linear distance of  $12.75 \pm 0.41$  Mpc. The resulting uncertainty of the distance determination consists of the very small internal TRGB measurement error of 0.007 mag, the calibration error of 0.02 mag, the foreground extinction inaccuracy in the direction of DDO 68 of 0.006 mag, and the aperture correction error of 0.05 mag. Our distance estimation is in excellent agreement with the measurement of [Cannon et al. \(2014\)](#) and within the errors of the data of [Sacchi et al. \(2016\)](#).

### 3.3 Stellar-population distribution

In Fig. 4, we present the density maps of four types of stellar populations in DDO 68. North is approximately to the right, East is up. The top panel shows the spatial distribution of the MS stars:  $F814W < 27.0$  and  $(F606W - F814W) < 0.6$ . The second top panel depicts the RSG:  $F814W < 25.5$  and  $(F606W - F814W) > 0.6$ . The next panel presents the AGB:  $25.5 < F814W < 26.4$  and  $(F606W - F814W) > 0.6$ . The bottom panel shows the distribution of the RGB:  $26.45 < F814W < 27.5$  and  $(F606W - F814W) > 0.6$ .

The difference in the distribution of the stellar populations of various ages is seen clearly. The young stars concentrate in several regions of active star formation. The most prominent burst coincides with the main body of DDO 68. As noted in [Pustilnik et al. \(2005\)](#), several prominent star formation regions are well-distinguished in the *HST*  $H\alpha$  image. They wind asymmetrically around the bright part of the galaxy and probably represent the tidal debris of a galaxy

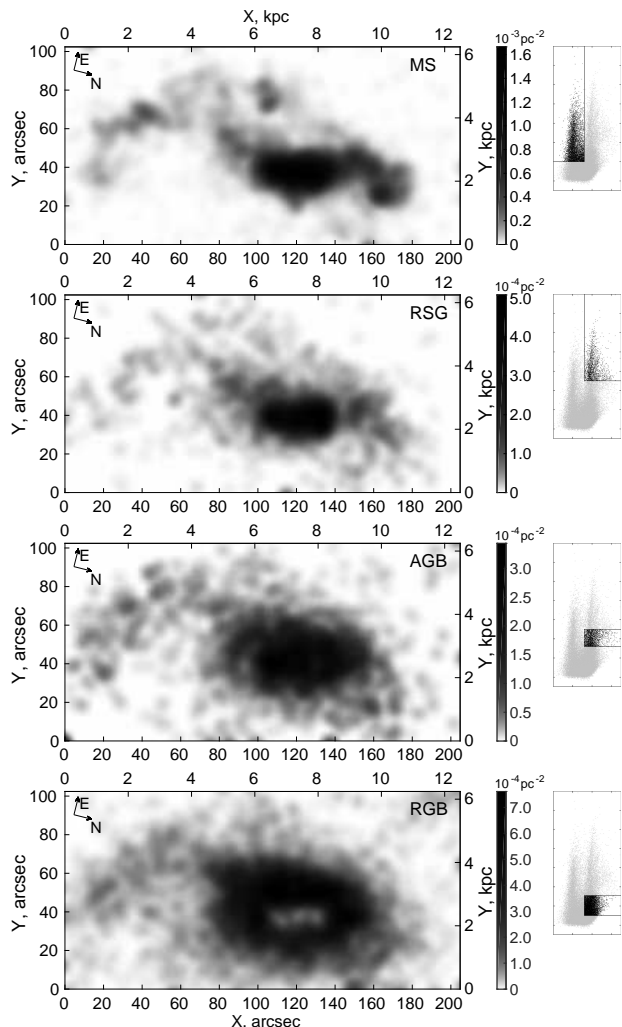


**Figure 4.** The maps of density distribution of the four different stellar populations. The top panel shows MS stars; the second top panel – RSG; the third one from the top – AGB stars; and the bottom panel – RGB population. The populations selected for the density maps are highlighted in the respective CMDs at the right.

minor merger. This morphology is clearly visible for all stellar populations, which favours its origin due to a recent interaction. Moreover, the MS stars show the distortion of the main body of DDO 68 connecting it with the ‘northern ring’ and the ‘southern tail’ regions (see Fig. 4). The distribution of RGB stars shows a ‘hole’ in the centre of DDO 68 due to the loss of stars in a crowded stellar field.

For the detailed analysis of different stellar populations, we selected several prominent regions of star formation using a hierarchical cluster tree from the sample of the bright blue part of the MS stars with  $(F606W - F814W) < 0.33$  and  $F814W < 26.5$  mag. These young stars depict the structures in DDO 68 more clearly. The result is shown in the Fig. 3. The selected regions are delineated by dashed lines. One can distinguish a conditional ‘arc’ of 7–8 regions with an overdensity of the blue MS stars. This ‘arc’ stretches asymmetrically beside the main body, starting from the ‘northern ring’ along the eastern edge of the ‘main body’ and continuing to the south as a ‘tail’. These structures

are clearly seen in the early images of DDO 68 and were used to classify this object as the interacting system VV 542 by [Vorontsov-Velyaminov \(1977\)](#). Taking into account the marked regions, we extracted for further analysis the next four groups of stars. These groups include all stars (not only young) within the areas enclosed by solid lines. The ‘body’ includes the galaxy centre (about 15000 stars). We divided the arc of starforming regions into the ‘head’ (about 3500 stars), which coincides with the ‘northern ring’, and the ‘tail’ (about 5600 stars), which includes most of the clumps. Also, we consider separately the ‘middle’ region (about 3500 stars) between the main body and the ‘tail’. It is rather well detached from the centre of the galaxy, but is probably not a simple extension of the ‘tail’.

### 3.4 SFH reconstruction

We derived the SFH of DDO 68 using the STARPROBE package ([Makarov & Makarova 2004](#)). The program develops an approximation to the observed distribution of stars in the CMD using the positive linear combination of synthetic diagrams formed by simple stellar populations (SSP: a set of single-age and single-metallicity populations). The details of our approach and the STARPROBE software are described by [Makarov & Makarova \(2004\)](#) and [Makarova et al. \(2010\)](#).

The observed data were binned into two-dimensional histograms (Hess diagrams) giving the number of stars in cells of the CMDs. The respective synthetic Hess diagrams were constructed from theoretical stellar isochrones and the adopted initial mass function (IMF). Each isochrone describes the magnitudes and colours of the SSP with the particular age and metallicity as a map of probabilities to find a star in each cell. We used the Padova2000 set of theoretical isochrones ([Girardi et al. 2000](#)), and a [Salpeter \(1955\)](#) IMF. The distance was adopted from this paper (see above) and the Galactic extinction is from [Schlegel et al. \(1998\)](#). The synthetic diagrams were altered by the same incompleteness and crowding effects and by photometric systematics identical to those determined for the observations using artificial stars experiments. We took into account the unresolved binary stars (binary fraction) to be 30 per cent. The mass function of the individual stars and the main components of binary systems was assumed to be the same. The mass distribution for the second components was taken to be flat in the range 0.7–1.0 of the main component mass. The synthetic diagrams covered the whole range of ages (from 4 Myr to 14 Gyr) and metallicities (from  $Z = 0.0001$  to 0.03). Hess diagrams of the SSP were combined together for a given time range under the assumption of a constant star formation rate (SFR) during this period (2-Gyr step for the populations older than 2 Gyr; 500-Myr step from 500 Myr to 2 Gyr; and 100-Myr step for populations younger than 500 Myr). The isochrones were interpolated in age to avoid discontinuities, so that the sampled points in the CMD were separated at most by 0.03 mag. The fitting procedure allowed us to use the boundaries of star formation episodes as free parameters of minimization. The metallicity resolution was limited by the underlying published isochrones; they were not interpolated in metallicity. As a result, we constructed a set of 60 synthetic Hess diagrams for seven predefined metallicities.

Using a stepwise approach, we selected only statistically significant episodes of star formation. It allowed us to avoid

problems with ‘noise’ from insignificant variables and improved the quality of the fit. At each iteration, we found an artificial diagram that correlated most strongly with the observational data, taking into account the variables already included in the regression. Using the partial Fisher criterion, a variable was included in the regression equation if its significance was greater than a pre-selected value. After that, the algorithm found a possibility to exclude previously selected variables from the resulting regression equation. We iterated until no more variables could be included in the regression. Therefore, this approach was purely statistical and did not impose any restrictions on the metallicity changes during the lifetime of a galaxy. It allowed us to analyse complex systems with an appearance of metal-poor populations in a merging process.

The best-fitting combination of the synthetic CMDs is a maximum-likelihood solution taking into account the Poisson noise of the star counts in the cells of the Hess diagram. The resulting SFH is illustrated in the Fig. 5. The  $1\sigma$  error of each SSP is derived from the analysis of the likelihood function.

According to our measurements, the large burst of star formation in this galaxy occurred during the period 12–14 Gyr ago. This initial burst accounts for 61 per cent of the total mass of the formed stars. Their estimated metallicity is quite low,  $[\text{Fe}/\text{H}]$  from  $-2$  to  $-1$ , and the mean SFR is  $7 \times 10^{-2} M_{\odot} \text{yr}^{-1}$ . We recognize only very slight traces of star formation during the periods of about 8–10, 4–6, and 1–2 Gyr ago. The detected metallicity of these stars is still low:  $[\text{Fe}/\text{H}] \sim [-2 : -1.6]$ . The enhanced star formation with a high rate of  $0.15 M_{\odot} \text{yr}^{-1}$  occurs in the last 300 Myr. The metallicity of these young stars of  $[-1; -0.5]$  is estimated with significant uncertainties due to their relatively low statistics. The estimated total stellar mass of DDO 68 is  $M = 1.8 \times 10^8 M_{\odot}$ .

Our results are in good agreement with [Sacchi et al. \(2016\)](#), who use a different methodology for SFH reconstruction. The figs 11–14 from their work show that recent star formation activity increases rapidly about 240–420 Myr ago with a peak between  $\sim 30$  and  $\sim 50$  Myr ago. The total stellar mass of young (age  $< 1$  Gyr) stars is about  $2.8\text{--}4.1 \times 10^7 M_{\odot}$ . This value is in good agreement with our estimation of  $3.2 \times 10^7 M_{\odot}$ .

It is worth comparing the SFH in the selected regions of DDO 68. We start from the ‘head’ region around the ‘northern ring’. There is no sign of ancient star formation. One can see only insignificant star formation about 8–10 Gyr ago. The metallicity of these stars is still within  $[\text{Fe}/\text{H}] = [-1 : -2]$ . According to our analysis in this area, there is no sign of middle-age stars. The modern episode of star formation is the most prominent in its history. Although it shows a lower rate than the galaxy as a whole ( $1.5 \times 10^{-2} M_{\odot} \text{yr}^{-1}$ ), the distribution of the ages and metallicities completely corresponds to it.

Three other regions (the ‘body’, the ‘middle’, and the ‘tail’) show the more or less oldest substantial episode of star formation in the period of 12–14 Gyr ago. The SFR in that epoch is comparable to the ongoing star formation only in the ‘middle’ region. In the ‘body’ and the ‘tail’, the SFR is significantly lower than the recent one. It is interesting to note that the estimated metallicity of the ancient stars varies from region to region. It is likely that all stars

in the ‘body’ have  $[\text{Fe}/\text{H}] = [-2.0 : -1.6]$ . In the ‘middle’ region, the fraction of stars with  $[\text{Fe}/\text{H}]$  from  $-1.6$  to  $-1.0$  is slightly higher than the population of the lower metallicity stars. Apparently, the oldest stars in the ‘tail’ have  $[\text{Fe}/\text{H}] = [-1.6 : -1.0]$ . Only two of the considered regions, the ‘middle’ and the ‘body’, show the faint traces of the middle-age stars. It is worth noting that the ongoing star formation episode (the last 300 Myr) is the most active in all considered regions, with a clear trend towards higher metallicity for most stars.

## 4 DISCUSSION

### 4.1 Old stellar population and its diversity in various parts of DDO 68

Our analysis of the CMD of DDO 68 and the SFH measurements shows a significant fraction of old giant stars in the ‘body’ region. The outer regions, the ‘head’ and the ‘tail’, show a higher fraction of young stars relative to the ‘body’ region. The main body, hosting a substantial amount of old stars, extends its population to the outer regions of DDO 68. The old stellar populations visible in the ‘head’ region could be explained by the contribution from the central region. Thus, we can conclude that the ‘head’ contains only bright and young MS stars. In the frame of the minor merger scenario, the ‘head’ region represents the remnant of a destroyed smaller gas-rich component. With its ‘young’ stellar populations and extremely low O/H, this destroyed dwarf is similar to other unusual dwarfs found in the void: J0926+3343 (Pustilnik et al. 2010), two faint low-surface-brightness dwarfs in the triplet J0723+36 (Chengalur & Pustilnik 2013), AGC 198691 (Hirschauer et al. 2016) and J0706+3620 (Pustilnik et al. 2016b).

The ‘tail’ region has both young and old stellar populations with an excess of MS stars compared to the ‘body’. The comparison of results for the two regions is evidence that the stellar population in the ‘tail’ is more evolved than in the ‘head’. Therefore, we can conclude that the star formation was induced during the pre-merger interaction in the ‘tail’ region, while the star formation burst in the ‘head’ ignited just recently. The more massive progenitor galaxy has a significant amount of the old stellar population. A part of this could be pulled out to the tidal ‘tail’. The smaller component of the merger was a gas-rich object with extremely low metallicity, as evidenced by the spectra of several young H II regions (Pustilnik et al. 2005; Izotov & Thuan 2007). Since the ongoing episode of star formation began about 300 Myr ago, we can suggest that the star formation burst marks the epoch of final coalescence of the merger components.

### 4.2 DDO 68 distance and the problem of large peculiar velocity

The new DDO 68 TRGB distance of  $12.75 \pm 0.41$  Mpc has an important implication. This distance is 2.85 Mpc larger than the adopted value by Pustilnik & Tepliakova (2011). The latter distance of 9.9 Mpc was obtained from the kinematic model of motion of galaxies in the vicinity of the Local Sheet due to its repulsion from the huge Local Void

(Tully et al. 2008). The distance estimation takes into account a large negative peculiar velocity in this sky area of  $\Delta V \approx -290 \text{ km s}^{-1}$ . The derived TRGB distance of DDO 68 implies an additional negative peculiar velocity of  $-208 \pm 30 \text{ km s}^{-1}$ . Hence the total negative peculiar velocity for this galaxy is about  $-500 \text{ km s}^{-1}$  (for the adopted Hubble constant  $H_0 = 73 \text{ km s}^{-1}$ ). The nature of this large negative peculiar velocity is unclear.

At the projected distances of 0.4–1.5 Mpc from DDO 68 there are six galaxies with very close radial velocities: J0926+3343 ( $V_{\text{hel}} = 536 \text{ km s}^{-1}$ ), KISSB 23 = J0940+2935 ( $V_{\text{hel}} = 505 \text{ km s}^{-1}$ ), UGC 5209 = J0945+3214 ( $V_{\text{hel}} = 538 \text{ km s}^{-1}$ ), UGC 5272 = J0950+3129 ( $V_{\text{hel}} = 520 \text{ km s}^{-1}$ ), J1000+3032 ( $V_{\text{hel}} = 484 \text{ km s}^{-1}$ ), and UGC 5427 = J1004+2921 ( $V_{\text{hel}} = 498 \text{ km s}^{-1}$ ). They form a filament with the projected length of  $\sim 9^\circ$ , which corresponds to 1.5–2.0 Mpc. The velocity independent distance determination of these galaxies is crucial to approve this great velocity anomaly and should help to understand its nature.

One could think that the Tully et al. (2008) kinematic model does not work properly in this region. However, the recent TRGB distance measurement of UGC 5209 (Karachentsev et al. 2015) is in good agreement with the model. The TRGB distance of UGC 5427 presented in the extragalactic distance data base (Jacobs et al. 2009) is lower than the model value. But a closer look at its CMD reveals probable confusion of RGB stars with the AGB population. After the proper correction, the *HST*-based distance of UGC 5427 also matches the kinematic model. The recent detailed theoretical analysis by Aragon-Calvo & Szalay (2013) shows that the velocity field in the void substructures on the scale of 1–2 Mpc is expected to be very smooth with variations less than  $20 \text{ km s}^{-1}$ . However, finding the smooth velocity flow and an abrupt jump in the distance of DDO 68 makes the task of independent distance determination for other galaxies in this region very important for understanding the kinematics of filaments in voids.

## 5 SUMMARY

Summarizing the results and discussion above, we draw the following conclusions:

(i) There is a clear dichotomy of the stellar content of DDO 68 between the bright main central body and the peripheral regions (including the ‘head’ and the ‘tail’). Apart from the large fraction of young populations, the ‘body’ also shows the prominent RGB. The outer regions display less significant fractions of old stars. Moreover, these old stars are probably interlopers (at least for ‘head’) from the outer parts of the main body. In the frame of this interpretation, the outer parts of DDO 68 represent a destroyed, smaller, gas-rich, and very low-metallicity galaxy in the process of an almost completed merger with a more massive and more typical dwarf.

(ii) The analysis of the SFH of DDO 68 shows that 61 per cent of the total stellar mass was formed during the initial burst of star formation in the epoch 12–14 Gyr ago. There are only weak traces of star formation in the period between 1 and 10 Gyr. The modern and ongoing star formation episode started about 300 Myr ago. It is characterized by the high mean rate of star formation  $\text{SFR} = 0.15 \text{ M}_\odot \text{ yr}^{-1}$ .

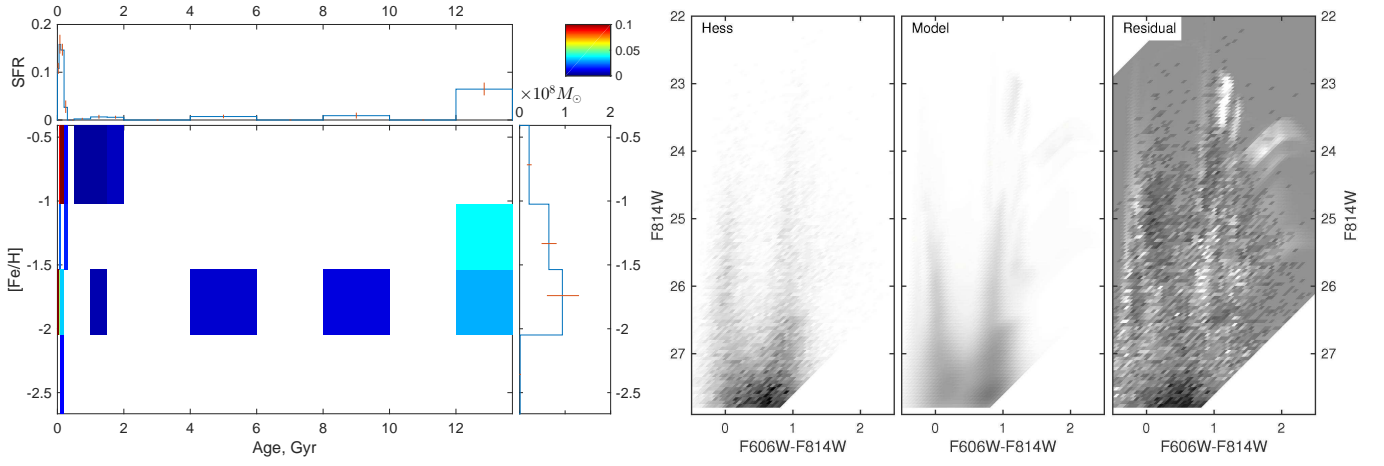


**Figure 5.** Left-hand set: the SFH reconstruction of DDO68. The measured SFR is coded with a colour (grey-scale) in the central panel against the respective age and metallicity. The top panel demonstrates the histogram of the SFR versus an age, and the left-hand panel shows the total mass fraction versus a metallicity. The error bars are  $1\sigma$  uncertainties of the maximum-likelihood estimation. Right-hand set: the Hess diagram of the resolved stars of DDO 68 is shown in the left-hand panel, and the best-fitting model Hess diagram is in the right-hand panel.

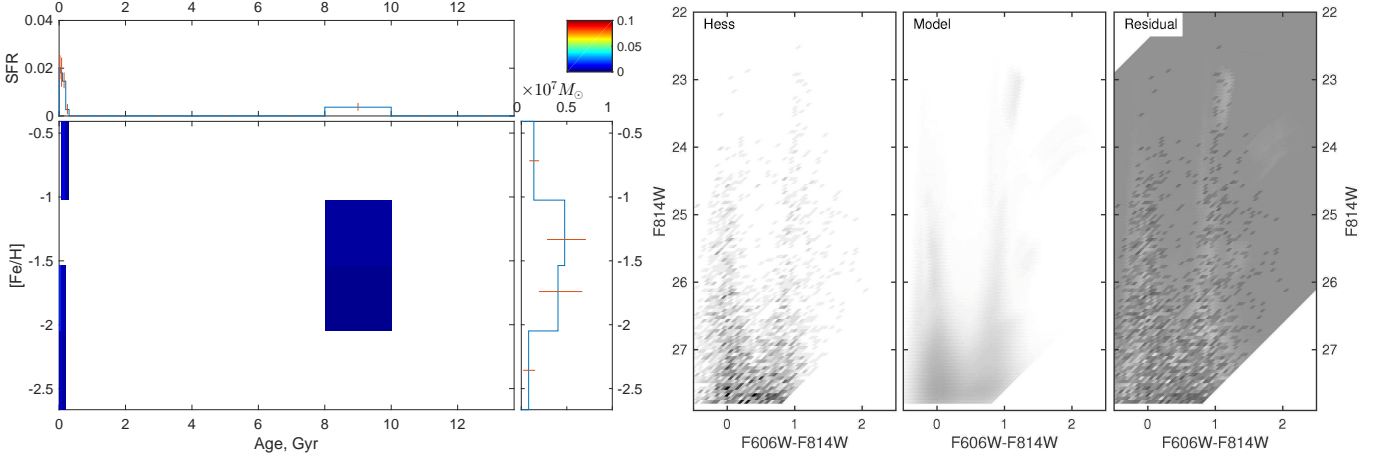


**Figure 6.** SFH reconstruction of ‘the head’ of DDO 68. The panels are organized as in Fig. 5.

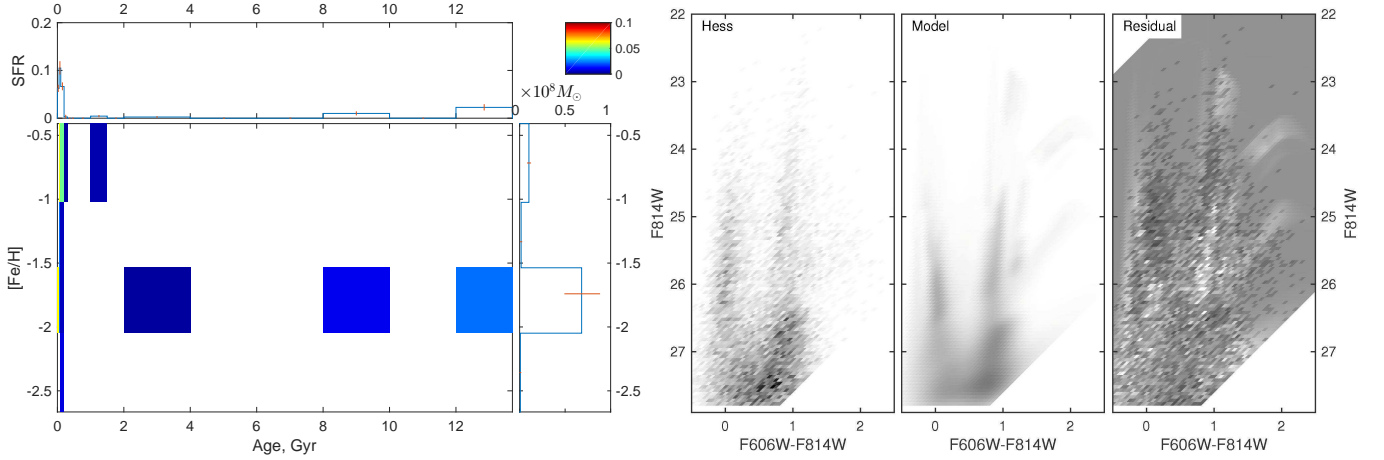


**Figure 7.** SFH reconstruction of ‘the body’ of DDO 68. The panels are organized as in Fig. 5.



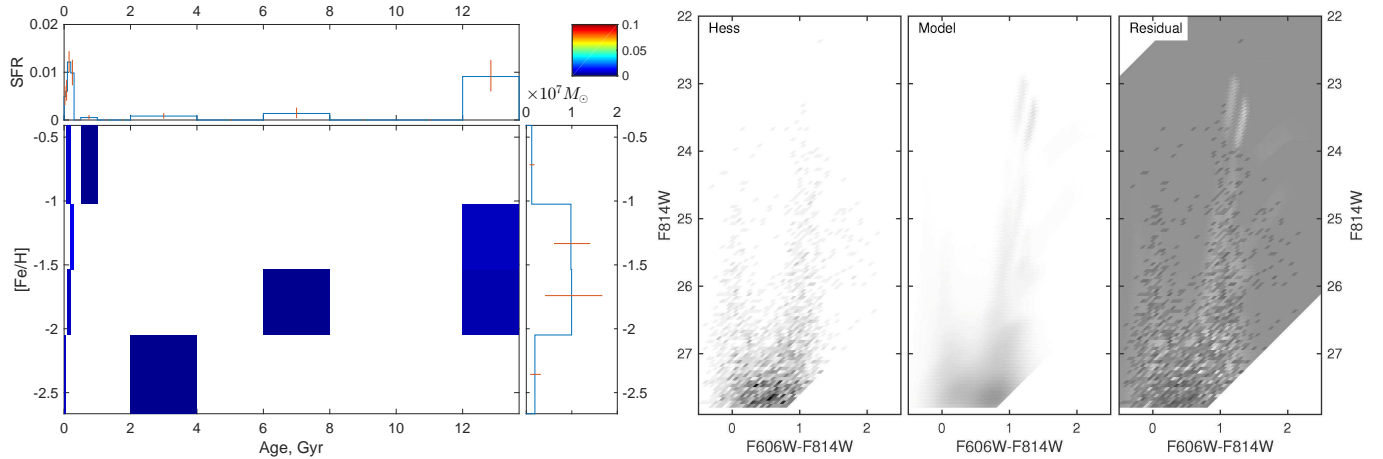


**Figure 8.** SFH reconstruction of ‘the middle’ of DDO 68. The panels are organized as in Fig. 5.

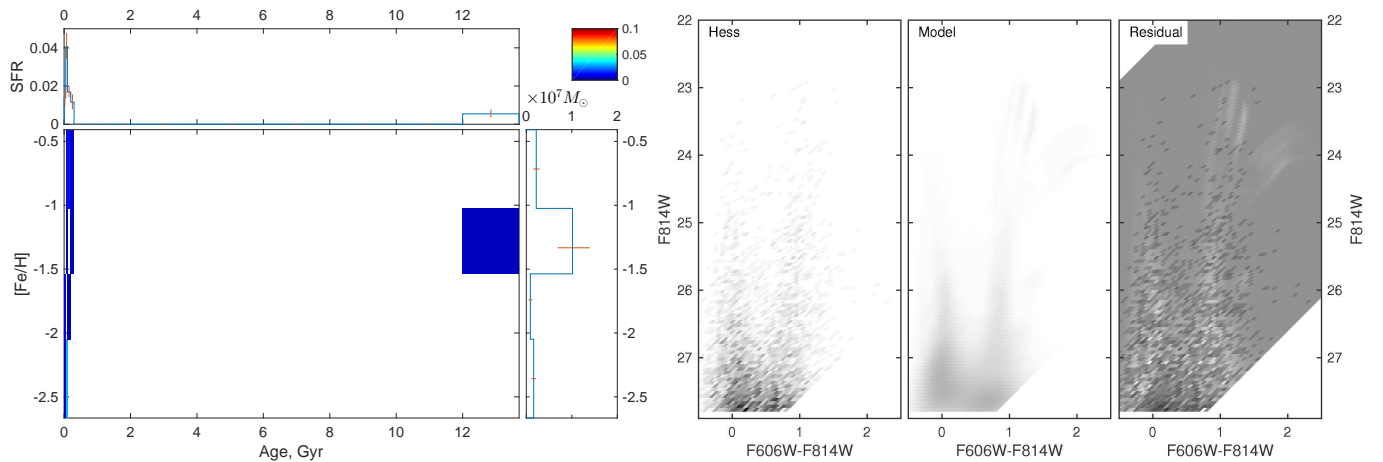


**Figure 9.** SFH reconstruction of ‘the tail’ of DDO 68. The panels are organized as in Fig. 5.

The great majority (80–88 per cent) of stars in the system as a whole are metal-poor, with  $Z = Z_{\odot}/50 - Z_{\odot}/20$ . Only  $\lesssim 20$  per cent of stars have  $Z \approx Z_{\odot}/5$ .

(iii) The new TRGB-based distance of DDO 68 is  $2.8 \pm 0.4$  Mpc farther relative to the previously adopted value from the kinematic model of Tully et al. (2008), which predicts a large negative peculiar velocity in this region of  $\Delta V \approx -290 \text{ km s}^{-1}$ . This result poses an important question on the origin of the additional peculiar velocity of  $\approx -200 \text{ km s}^{-1}$  of DDO 68, which, if real, implies a value of the peculiar velocity of  $\approx -500 \text{ km s}^{-1}$  in this region.

## ACKNOWLEDGEMENTS

This article is based on archival data of the Space Telescope Science Institute (STScI) obtained with the NASA/ESA *Hubble Space Telescope*, programme GO-11578. The STScI is operated by the Association of Universities for Research in Astronomy, Inc. under NASA contract NAS 5-26555. This work was carried out with the support of the Russian Science Foundation grant 14-12-00965 (distance and structure of DDO 68). LNM acknowledges the support of Research Program OFN-17 of the Division of Physics, Russian Academy

of Sciences (SFH reconstruction). The authors thank N. A. Tikhonov, who kindly made available his and his co-authors’ paper prior to publication.

## REFERENCES

- Annibali F., et al., 2016, *ApJ*, **826**, L27  
 Aragon-Calvo M. A., Szalay A. S., 2013, *MNRAS*, **428**, 3409  
 Bellazzini M., Ferraro F. R., Sollima A., Pancino E., Origlia L., 2004, *A&A*, **424**, 199  
 Berg D. A., et al., 2012, *ApJ*, **754**, 98  
 Cannon J. M., et al., 2014, *ApJ*, **787**, L1  
 Chengalur J. N., Pustilnik S. A., 2013, *MNRAS*, **428**, 1579  
 Chengalur J. N., Pustilnik S. A., Egorova E. S., 2016, preprint, ([arXiv:1611.01271](https://arxiv.org/abs/1611.01271))  
 Contreras Ramos R., et al., 2011, *ApJ*, **739**, 74  
 Dolphin A. E., 2002, *MNRAS*, **332**, 91  
 Ekta, Chengalur J. N., Pustilnik S. A., 2008, *MNRAS*, **391**, 881  
 Girardi L., Bressan A., Bertelli G., Chiosi C., 2000, *A&AS*, **141**, 371  
 Haynes M. P., et al., 2011, *AJ*, **142**, 170  
 Hirschauer A. S., et al., 2016, *ApJ*, **822**, 108  
 Izotov Y. I., Thuan T. X., 1998, *ApJ*, **497**, 227  
 Izotov Y. I., Thuan T. X., 2004, *ApJ*, **616**, 768  
 Izotov Y. I., Thuan T. X., 2007, *ApJ*, **665**, 1115



- Izotov Y. I., Thuan T. X., 2009, *ApJ*, **690**, 1797
- Izotov Y. I., Guseva N. G., Fricke K. J., Papaderos P., 2009, *A&A*, **503**, 61
- Izotov Y. I., Thuan T. X., Guseva N. G., 2012, *A&A*, **546**, A122
- Jacobs B. A., Rizzi L., Tully R. B., Shaya E. J., Makarov D. I., Makarova L., 2009, *AJ*, **138**, 332
- Karachentsev I. D., Tully R. B., Makarova L. N., Makarov D. I., Rizzi L., 2015, *ApJ*, **805**, 144
- Lee M. G., Freedman W. L., Madore B. F., 1993, *ApJ*, **417**, 553
- Makarov D. I., Makarova L. N., 2004, *Astrophysics*, **47**, 229
- Makarov D., Makarova L., Rizzi L., Tully R. B., Dolphin A. E., Sakai S., Shaya E. J., 2006, *AJ*, **132**, 2729
- Makarova L. N., Karachentsev I. D., 1998, *A&AS*, **133**, 181
- Makarova L., Koleva M., Makarov D., Prugniel P., 2010, *MNRAS*, **406**, 1152
- Pustilnik S. A., Tepliakova A. L., 2011, *MNRAS*, **415**, 1188
- Pustilnik S. A., Kniazev A. Y., Pramskij A. G., 2005, *A&A*, **443**, 91
- Pustilnik S. A., Tepliakova A. L., Kniazev A. Y., Burenkov A. N., 2008, *MNRAS*, **388**, L24
- Pustilnik S. A., Tepliakova A. L., Kniazev A. Y., Martin J.-M., Burenkov A. N., 2010, *MNRAS*, **401**, 333
- Pustilnik S. A., Makarova L. N., Perepelitsyna Y. A., Moiseev A. V., Makarov D. I., 2016a, preprint, ([arXiv:1611.08489](https://arxiv.org/abs/1611.08489))
- Pustilnik S. A., Perepelitsyna Y. A., Kniazev A. Y., 2016b, *MNRAS*, **463**, 670
- Rizzi L., Tully R. B., Makarov D., Makarova L., Dolphin A. E., Sakai S., Shaya E. J., 2007, *ApJ*, **661**, 815
- Sacchi E., et al., 2016, *ApJ*, **830**, 3
- Salpeter E. E., 1955, *ApJ*, **121**, 161
- Schlegel D. J., Finkbeiner D. P., Davis M., 1998, *ApJ*, **500**, 525
- Skillman E. D., Kennicutt Jr. R. C., 1993, *ApJ*, **411**, 655
- Skillman E. D., et al., 2013, *AJ*, **146**, 3
- Stil J. M., Israel F. P., 2002, *A&A*, **389**, 29
- Tikhonov N. A., Galazutdinova O. A., Lebedev V. S., 2014, *Astronomy Letters*, **40**, 1
- Tully R. B., Shaya E. J., Karachentsev I. D., Courtois H. M., Kocevski D. D., Rizzi L., Peel A., 2008, *ApJ*, **676**, 184
- Vorontsov-Velyaminov B. A., 1977, *A&AS*, **28**, 1

This paper has been typeset from a  $\text{\TeX}/\text{\LaTeX}$  file prepared by the author.